ACCSCIENCE PUBLISHING

International Journal of Bioprinting

RESEARCH ARTICLE

Optimization of alginate/gelatin/dextran-aldehyde bioink for 3D bioprinting and cell engraftment

Hosub Lim[1†], Daun Seo[2†], Kyung Deok Park[1], Hye-Eun Shim[3], Ji Hye Park[3], Eun-Jung Ann[3], Junghyun Kim[2], Jae Young Lee[2*], Junhee Lee[1*], and Sun-Woong Kang[3,4*]

[1]Department of Bionic Machinery, Research Institute of AI Robotics, Korea Institute of Machinery & Materials, Daejeon, Republic of Korea

[2]School of Materials Science and Engineering, Gwangju Institute of Science and Technology, Gwangju, Republic of Korea

[3]Center for Biomimetic Technology Research, Korea Institute of Toxicology, Daejeon, Republic of Korea

[4]School of Korea Institute of Toxicology, University of Science and Technology, Daejeon, Republic of Korea

(This article belongs to the *Special Issue: Bioprinting for Tissue Engineering and Modeling*)

[†]These authors contributed equally to this work.

***Corresponding authors:**
Sun-Woong Kang (swkang@kitox.re.kr)

Junhee Lee (meek@kimm.re.kr)

Jae Young Lee (jaeyounglee@gist.ac.kr)

Citation: Lim H, Seo D, Park KD, *et al*. Optimization of alginate/gelatin/dextran-aldehyde bioink for 3D bioprinting and cell engraftment. *Int J Bioprint*. 2025;11(3):241-260. doi: 10.36922/ijb.8440

Received: January 7, 2025
1st revised date: February 25, 2025
2nd revised date: March 18, 2025
3rd revised date: March 26, 2025
Accepted: March 26, 2025
Published online: March 26, 2025

Abstract

The development of bioinks with optimized printability, mechanical properties, and biocompatibility is critical for advancing three-dimensional (3D) bioprinting and tissue engineering. In this study, we introduce an alginate/gelatin/dextran-aldehyde (AGDA) bioink, designed to balance structural integrity and cellular functionality. Among the tested formulations, AGDA1 demonstrated superior performance, with optimized printability and high cell compatibility. AGDA bioinks involve dual crosslinking (ionic gelation of alginate and Schiff base formation between gelatin and dextran-aldehyde), permitting appropriate stiffness, viscosity, and thixotropic behavior. Fibroblasts encapsulated in AGDA, either as single cells, spheroids, or a combination of both, exhibited high viability and proliferative capacity. Notably, the combination method supported the highest cellular density and fibroblast-specific morphological transformations, surpassing the commercially available GelXA bioink. These findings highlight AGDA's potential as a versatile bioink for fabricating complex and scalable tissue constructs. In summary, this study contributes to the development of bioinks tailored for enhanced cell engraftment and regenerative applications.

Keywords: Bioink; Bioprinting; Dual crosslinking; Spheroid; Tissue engineering

1. Introduction

Three-dimensional (3D) bioprinting has emerged as a transformative technology in tissue engineering and regenerative medicine, enabling the fabrication of complex, biomimetic tissue constructs through the precise deposition of bioinks.[1–6] A critical factor determining the success of 3D bioprinting is the design and optimization of bioinks that

exhibit both excellent printability and biocompatibility.[4–6] Bioinks must offer structural stability during and after printing and a supportive microenvironment for cell survival, proliferation, and function. Despite significant advancements, the development of functional bioink formulations and cell encapsulation methods remains a critical challenge, particularly for enhancing cell survival, engraftment, and functionality for tissue regeneration applications.

Hydrogel-based bioinks, commonly composed of natural polymers, such as alginate,[7–12] gelatin,[12–15] and dextran derivatives,[15–17] are widely utilized due to their biocompatibility and tunable physicochemical properties. Alginate, a natural polysaccharide, provides rapid ionic crosslinking when exposed to divalent cations such as calcium, which stabilizes printed structures.[7,8] However, alginate alone lacks bioactive motifs for cell adhesion and often results in brittle hydrogels post-crosslinking, potentially compromising mechanical stability and cell functionality.[11,12] Therefore, researchers often blend alginate with other polymers or modify its structure to improve printability and mechanical properties. Gelatin, derived from collagen, enhances cell adhesion, proliferation, and differentiation by mimicking key features of the extracellular matrix (ECM).[12,13] It also contributes to the thermoresponsive behavior of bioinks, aiding the extrusion process during bioprinting. Dextran-aldehyde, a chemically modified natural polymer, introduces additional crosslinking potential and enhances the mechanical and cohesion properties of hydrogels through Schiff base formation with gelatin, leading to a dual crosslinked network that offers tunable stiffness and viscosity.[14,18–20] In the context of printability, bioinks must demonstrate shear-thinning behavior, high shape fidelity post-printing, and adequate mechanical strength to support complex 3D structures.[21,22] Various criteria, including filament formation, layer stacking ability, and structural stability under physiological conditions, are used to evaluate and optimize bioink printability. Previous studies have shown that balancing the viscoelastic properties of bioinks is crucial for achieving both high print fidelity and cell viability.[7–17]

The method of cell encapsulation within bioinks also plays a critical role in tissue regeneration.[5,6] Single-cell encapsulation is widely used due to its simplicity and ability to distribute cells evenly throughout constructs.[23,24] However, single cells alone may lack the intercellular interactions and microenvironmental cues necessary to fully replicate native tissue functionality. Spheroid-based encapsulation, by contrast, provides pre-formed 3D cellular aggregates that closely mimic native tissue microenvironments.[25–28] After encapsulation within hydrogels, spheroids must not merely retain their aggregate form but instead become activated. This activation involves promoting their engraftment within the bioink matrix, enhancing their interactions with surrounding cells, and creating an environment that maximizes their functional capacity.[6,21,22] Designing bioinks that support such dynamic cellular processes while maintaining the structural integrity of the printed construct remains a significant challenge. Comprehensive research is still needed to achieve the highest survival, activation, and transplantation rates through encapsulation methods that can integrate the structural advantages of single cells and the functional advantages of spheroids within bioinks.

In this study, we aimed to develop and optimize a printable bioink composed of dextran-aldehyde, gelatin, and alginate crosslinked with $CaCl_2$ (Figure 1). We systematically examined its printability and compared the following three cell encapsulation strategies: single cells, spheroids, and a combination of the two. Through the analysis of cell survival and engraftment rates, we sought to identify the optimal bioink formulation and encapsulation method for tissue engineering applications, contributing valuable insights into bioink design and encapsulation techniques to advance the field of 3D bioprinting.

2. Materials and Methods

2.1. Materials

Sodium alginate (Cat No. A2033, medium viscosity, mannuronic acid to guluronic acid ratio = 1.56, molecular weight range of 120,000–190,000 Da), gelatin from porcine skin (gel strength ~300 g bloom, type A), dextran from *Leuconostoc* spp. (average molecular weight 450,000–650,000 Da), sodium periodate ($NaIO_4$), ethylene glycol, hydroxylamine hydrochloride ($NH_2OH{\cdot}HCl$), deuterium oxide, sodium bicarbonate ($NaHCO_3$), sodium dodecyl sulfate (SDS), and glycine were purchased from Sigma-Aldrich (St. Louis, MO, USA). All reagents were used without further purification. Deionized (DI) water was used for all solution preparations and experiments.

GelXA bioink (Cat No. IK3X2102, CELLINK, Sweden) is a semi-translucent gel based on gelatin methacrylate (GelMA) incorporating xanthan gum and alginate to enhance printability, ease-of-use, and stability post-printing. It offers dual-crosslinking capabilities through photocuring and treatment with the included crosslinking agent. GelXA bioink has a GelMA degree of methacrylation in the range of 45–55%, a gelation temperature of 23–27 °C, and viscosity in the range of 90–350 Pa·s.[29]

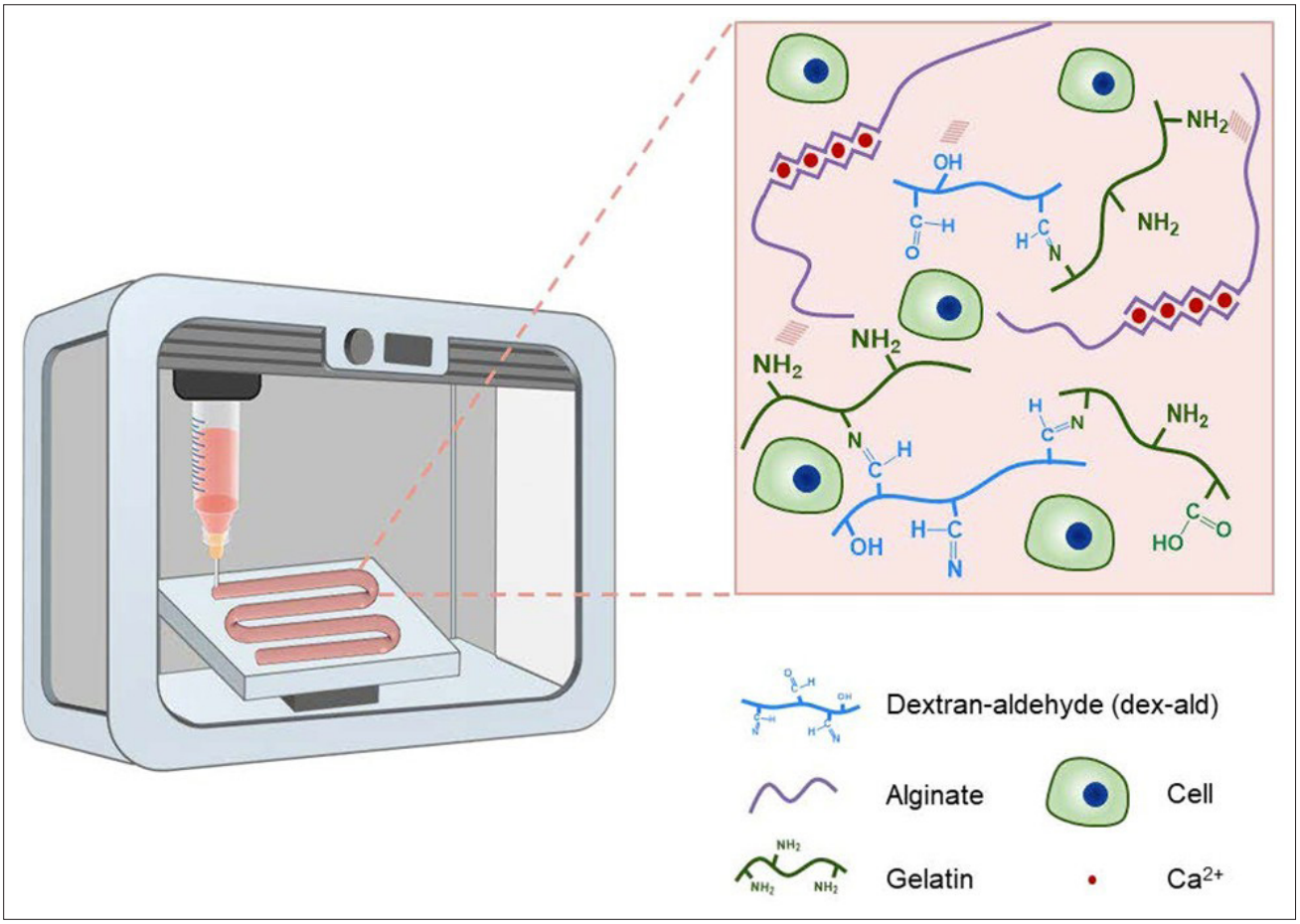

Figure 1. Schematic representation of the AGDA bioink components and crosslinking mechanisms. Alginate undergoes ionic crosslinking with calcium ions, while gelatin forms Schiff base linkages with dextran-aldehyde, providing the bioink with sufficient mechanical properties and printability for 3D bioprinting applications. Abbreviation: AGDA, alginate/gelatin/dextran-aldehyde.

2.2. Synthesis and characterization of dextran-aldehyde

2.2.1. Synthesis of dextran-aldehyde

Dextran-aldehyde (dex-ald) was synthesized via oxidation of dextran following previously established protocols.[30] Briefly, 5 g of dextran was dissolved in 500 mL of DI water at 25 °C with stirring. Sodium periodate (2.673 g) was dissolved in 20 mL of DI water and added dropwise to the dextran solution with vigorous stirring in the dark at 25 °C for 2 h. The oxidation reaction was terminated by adding 0.695 mL of ethylene glycol, followed by an additional hour of stirring. The resulting solution was dialyzed against DI water for 4 days using a 3500 Da molecular weight cut-off membrane (Spectrum Laboratories, Inc., TX, USA). After dialysis, the solution was filtered through a 0.2 μm filter and freeze-dried to obtain dex-ald powder.

2.2.2. Characterization of dextran-aldehyde

The aldehyde content of dex-ald was determined using hydroxylamine hydrochloride titration. Dex-ald (0.1 g) was dissolved in 10 mL of 25 mM $NH_2OH{\cdot}HCl$ solution and incubated for 1 h. The solution was titrated with 0.1 M NaOH, and the aldehyde group concentration was calculated to be 3.48 mmol/g, corresponding to a degree of substitution of 58.5%.

Spectroscopic methods were used to confirm the chemical structure of dex-ald. Proton nuclear magnetic resonance (^{1}H NMR) spectra of dextran and dex-ald were acquired using an Avance Neo 600 MHz NMR spectrometer (Bruker, Germany) in deuterium oxide at 10 mg/mL. Fourier-transform infrared spectroscopy (FTIR) was performed using a Vertex 70v/Hyperion 2000 FTIR spectrometer (Bruker, USA). The spectral data were collected in the range of 600–4000 cm^{-1} with a resolution of 4 cm^{-1}, and an average infrared (IR) spectrum

for each sample was obtained by performing 64 scans at room temperature.

The molecular weights (Mw) and polydispersity indices (PDI) of alginate, dextran, dex-ald, and gelatin were analyzed using gel permeation chromatography (GPC) coupled with a multi-angle light scattering detector (miniDAWN TREOS, Wyatt Technology Co., CA, USA) and a refractive index detector (RI2012A, Schambeck SFD, Germany) (Table S1, Supporting Information).

2.2.3. Quantification of amine groups in gelatin

The amine content of gelatin was quantified using a trinitrobenzene sulfonic acid (TNBSA) assay. Gelatin (20 μg/mL) was dissolved in 0.1 M sodium bicarbonate buffer (pH 8.5). A series of glycine standards (0.625–20 μg/mL) was prepared for calibration. TNBSA was diluted to 0.01% in sodium bicarbonate buffer and mixed with 0.5 mL of sample or standard. After 2 h of incubation at 37 °C with shaking, 0.25 mL of 10% SDS and 0.125 mL of 1 M HCl were added to terminate the reaction. Absorbance was measured at 335 nm using a UV–vis spectrophotometer (Touch Duo, Biodrop, Cambridge, UK).

2.3. Preparation and characterization of bioinks

2.3.1. Preparation of bioinks

Dex-ald solution (10 wt%) was prepared in 0.15 M NaCl containing 3.33% 0.1 M NaOH at 37 °C. Separately, 20 wt% gelatin and 2 wt% alginate solutions were prepared in 0.15 M NaCl at 37 °C. The alginate and gelatin solutions were combined in a 3:1 ratio using a syringe mixer (NOBAMEDI CO., LTD., Yongin-si, Republic of Korea). The dex-ald and 1.12 wt% $CaCl_2$ solutions were then mixed with the alginate-gelatin blend to obtain final bioink formulations with varying dex-ald concentrations (Table 1).

2.3.2. Mechanical properties of bioinks

The mechanical properties of alginate/gelatin/dextran-aldehyde (AGDA) bioinks were analyzed using an oscillatory rheometer (Kinexus, Malvern Instruments, UK) following previously established protocols.[24] The storage modulus (G') and loss modulus (G'') were measured at a frequency of 1 Hz and a strain of 0.5% at 4 °C for 20 min, followed by 25 °C for 20–80 min using plate geometry with a 1.0 mm gap and 15 mm diameter. The viscosity of each bioink was measured at 25 °C under a shear rate range of 0.1–100 s^{-1} at 30 and 70 min after mixing. Changes in shear modulus and viscosity were expressed as percentage changes (%), calculated using the following formula:

$$\text{Change}(\%) = \frac{\text{Value at 70 min} - \text{Value at 30 min}}{\text{Value at 30 min}} \times 100 \quad \text{(I)}$$

Table 1. Nomenclatures and compositions of various AGDA bioinks.

Group name	Alginate (% w/v)	Gelatin (% w/v)	Dex-ald (% w/v)	$CaCl_2$ (% w/v)
$AGDA_0$	1	3	0	0.05
$AGDA_1$	1	3	1	0.05
$AGDA_2$	1	3	2	0.05
$AGDA_3$	1	3	3	0.05

Abbreviation: AGDA, alginate/gelatin/dextran-aldehyde; Dex-ald, dextran-aldehyde.

Thixotropic behavior was assessed by alternating shear rates between 0.1 and 50 s^{-1} for intervals of 180 s, with viscosity recovery analyzed after each cycle.

2.3.3. Cell cytotoxicity assessment

The potential cytotoxicity of the AGDA bioinks was evaluated based on the ISO 10993-5 standard established by the International Organization for Standardization (ISO). This assessment was conducted using human dermal fibroblasts (HDFs) as the primary cell type and further validated with skeletal muscle cells. Cells were seeded at a density of 2×10^5 cells/well in 6-well culture plates (Corning, USA) and incubated at 37 °C in a humidified atmosphere containing 5% CO_2 for 48 h. After the initial incubation, AGDA bioink samples (1×1 cm^2) were placed directly in the center of each well, allowing direct contact with the cells. The cells were cultured for an additional 3 days under the same conditions. For comparison, a positive control group utilized polyetherurethane film containing 0.1% zinc diethyldithiocarbamate (PU-ZDEC, Hatano Research Institute, Japan), a material known to induce cytotoxicity. The cytotoxic response was quantified by measuring the size of the toxic reaction zone using ImageJ software (National Institutes of Health, USA). The degree of cytotoxicity was classified according to established criteria outlined in Table 2. The quantitative analysis of cell viability was performed for both cell types under encapsulation conditions. Live/Dead assays (Invitrogen, USA) were conducted on days 1 and 3 to evaluate cell viability and death. Fluorescence imaging was performed using a DMi8 fluorescence microscope (Leica, Germany), and the results were analyzed for improved clarity. Cell viability was quantified by counting live (green) and dead (red) cells across multiple fields of view ($n = 5$ per sample) using ImageJ software. The percentage of live cells relative to the total cell population was calculated.

2.3.4. Cell affinity assessment

The cell affinity of AGDA bioinks was evaluated using fibroblasts encapsulated within the bioinks (human

Table 2. Chemical compositions of bioink

Grade	Reactivity	Description of reactivity zone
0	None	No detectable zone around or under specimen
1	Slight	Zone limited to area under specimen
2	Mild	Zone extends less than 0.5 cm beyond specimen
3	Moderate	Zone extends 0.5–1.0 cm beyond specimen
4	Severe	Zone extends greater than 1.0 cm beyond the specimen but does not involve entire dish

primary dermal fibroblast; PCS-201-012, ATCC, USA). This evaluation aimed to determine the biocompatibility of the bioinks and their potential for tissue engineering applications. The procedure followed was similar to the cytotoxicity assessment, with modifications to incorporate encapsulation. Fibroblasts were encapsulated within the bioinks at a concentration of 6×10^6 cells/mL in 6-well culture plates (Corning, USA) and incubated at 37 °C in a humidified atmosphere containing 5% CO_2. Various AGDA bioink formulations (AGDA0, AGDA1, AGDA2, AGDA3) were prepared and added to the culture medium. The cells were cultured for 5 days, and cell viability was analyzed on days 3 using a Live/Dead assay (Invitrogen, USA), following the manufacturer's protocol.

2.4. Printability assessment

All bioprinting experiments were conducted using a PROTEK 3D bioprinter (Korea Institute of Machinery and Materials, Daejeon, Republic of Korea). Prior to bioprinting, all equipment was sterilized under ultraviolet (UV) light. The bioprinter consisted of three pneumatic-driven dispensers mounted on three-axis automatic stages, which were controlled by customized Bioplot software (Republic of Korea). For the experiments, HDFs(PCS-201-012, ATCC, USA) and spheroids were encapsulated in the optimized AGDA1 bioink at concentrations of 2×10^6 cells/mL and 6000 spheroids/mL, respectively.

The printing process was performed at a controlled temperature of 20 °C for both the bioprinter and the dispensing nozzle. The bioink was extruded through a 22 G nozzle with an inner diameter of 420 μm. The nozzle dimension (22G) was selected based on its suitability for spheroid printing. The average spheroid size in our experiments was approximately 120 μm, and 22G was the optimal nozzle size to allow smooth extrusion without clogging while maintaining structural fidelity.[31,32] While larger nozzle sizes could also accommodate spheroid printing, they may compromise the precision of printed structures. Therefore, we used a 22G nozzle in this study to balance spheroid extrusion efficiency and print resolution. The printing feed rates ranged from 600 to 1600 mm/min, and the pneumatic pressure was adjusted between 120 and 280 kPa to achieve optimal print fidelity. The layer height was set at 0.4 mm for the first layer and 0.37 mm for subsequent layers to account for bioink spreading.

Print fidelity was assessed using the following criteria: (1) line resolution, defined by the consistency of filament width compared to the nozzle diameter; (2) shape fidelity, evaluated by the accuracy of printed structures against digital models; and (3) structural stability, determined by the ability of constructs to maintain their shape during and after bioprinting. All layers were printed in a serpentine configuration with a grid pitch of 0.5 mm for cell-laden bioinks and 0.125 mm for spheroid-laden bioinks, with a total grid length of 10 mm. The layered cuboid constructs were designed using Bioplot software, which also controlled the printing paths. After bioprinting, the constructs were temporarily immersed in Dulbecco's Modified Eagle Medium (DMEM) and stored in a humidified incubator at 37 °C with 5% CO_2 until further use.

2.5. Preparation of spheroids

Spheroids were generated using ultra-low attachment (ULA) culture dishes with integrated mesh (35 mm; LabToLab Co., Republic of Korea), specifically designed to prevent cell adhesion and promote uniform spheroid size. Adherent cells were harvested from monolayer cultures by enzymatic detachment with trypsin-EDTA, followed by centrifugation at 300 ×*g* for 5 min. The cell pellet was resuspended in fresh culture medium to achieve a final density of 1×10^6 cells/mL. A total volume of 1 mL of the single-cell suspension was seeded into each ULA dish. Cultures were maintained in growth medium specific to the fibroblasts, with 50% of the medium replaced every 48 h to ensure a consistent nutrient supply while minimizing disturbance to spheroid formation. Spheroid growth and morphology were monitored daily using an optical microscope (Leica DMi8, Germany). The size and uniformity of the spheroids were documented using calibrated imaging software.

2.6. Evaluation of cell survival and morphological changes

The long-term survival, morphological changes, and proliferation of fibroblasts encapsulated in AGDA1 bioink were assessed using the following three encapsulation methods: single cells, spheroids, and a combination of both. The commercially available GelXA bioink was used as a control for comparative analysis due to its dual crosslinking mechanism, which is similar to that of the

DGDA bioink. Additionally, GelXA contains gelatin methacrylate, xanthan gum, and alginate, providing comparable core components to AGDA1, thereby offering a relevant benchmark for evaluating printability, mechanical properties, and biocompatibility under consistent experimental conditions.

2.6.1. Encapsulation of fibroblasts in bioinks

Fibroblasts were encapsulated in AGDA1 and GelXA bioinks to maintain a consistent total cell density of 2×10^6 cells/mL across all experimental conditions. The single-cell suspension method involved directly mixing 2×10^6 fibroblasts/mL into the bioink, while the spheroid encapsulation method utilized approximately 6000 spheroids/mL, with each spheroid containing 330–340 cells to achieve the target cell concentration. For the combination method, a mixture of 1×10^6 single cells/mL and 3000 spheroids/mL was used, ensuring that the total cell concentration remained 2×10^6 cells/mL. Encapsulation was performed by gently mixing cells or spheroids with the prepared bioinks at 37 °C before loading into molds for bioprinting and constructs were printed in a cuboid configuration ($10 \times 10 \times 2$ mm^3) using a PROTEK 3D bioprinter under optimized printing conditions. This approach maintained consistent cell densities while accounting for the differences in visual distribution between single cells and spheroids due to their structural characteristics.

2.6.2. Culture conditions

The encapsulated constructs were transferred to 6-well plates (Corning, USA) and immersed in DMEM (Gibco, USA) supplemented with 10% fetal bovine serum (FBS) and 1% penicillin-streptomycin. Constructs were cultured at 37 °C in a humidified atmosphere containing 5% CO_2 for up to 14 days. The medium was replaced every 48 h to ensure a consistent nutrient supply.

2.6.3. Live/Dead staining and imaging

Cell viability was assessed using a Live/Dead assay kit (Invitrogen, USA) on days 1, 7, and 14. Constructs were washed with phosphate-buffered saline (PBS) and incubated with Calcein-AM (2 μM) and ethidium homodimer-1 (4 μM) for 30 min at 37 °C. Fluorescent images were captured using a Leica DMi8 fluorescence microscope (Germany) to visualize viable (green) and dead (red) cells.

2.6.4. Morphological observation and cellular density analysis

The morphology of encapsulated cells was monitored using phase-contrast microscopy (Leica DMi8, Germany) on days 1, 7, and 14. Morphological changes, including the transition from rounded to spindle-shaped fibroblasts, were documented. Quantitative analysis of cellular density within the bioinks was performed using ImageJ software. Cellular density was calculated as the total area of viable cells per unit area of the construct at each time point.

2.7. Statistical analysis

All experiments were conducted in triplicate. Quantitative data were expressed as mean ± standard deviation. Statistical significance between groups was determined using one-way analysis of variance (ANOVA) followed by Tukey's post hoc test, with a p-value of <0.05 considered statistically significant.

3. Results

3.1.1. Synthesis of AGDA bioinks

The chemical modification of dextran to dex-ald was confirmed using both spectroscopic and quantitative analyses. Figure 2A presents the proton nuclear magnetic resonance (^{1}H NMR) spectra of unmodified dextran and dex-ald. Chemical shifts in the range of 3.1–3.8 ppm were attributed to the protons of the glucopyranosyl rings in the dextran monomer units. However, the characteristic aldehyde proton peaks typically appearing between 9.0 and 9.5 ppm were not detected in the dex-ald spectrum, likely due to the reaction between aldehyde groups and neighboring hydroxyl groups, resulting in the formation of hemiacetal or hemialdal linkages. The presence of multiple peaks between 4.0 and 5.5 ppm further supports the formation of hemiacetal structures during the oxidation process. These findings confirm the successful oxidation of dextran and the introduction of aldehyde groups to form dex-ald.

FTIR spectra of the samples revealed characteristic absorption bands and their corresponding molecular vibrations (Figure 2B). The broad band at 3340 cm^{-1} is attributed to the stretching vibration of hydroxyl (–OH) groups, while the peak at 2918 cm^{-1} corresponds to the C–H stretching vibration. The absorption band at 1153 cm^{-1} is associated with C–O–C and C–O bonds at the C4 position of glucose units, and the peak at 1001 cm^{-1} indicates the α-glycosidic bonds characteristic of the polysaccharide backbone. Importantly, the spectrum of dex-ald exhibited a distinct aldehyde-specific peak at 1733 cm^{-1}, corresponding to the C=O stretching vibration. This peak, marked with a blue arrow for clarity, was absent in the native dextran spectrum, providing robust evidence of successful aldehydic modification. Additional analysis of the FTIR region between 2830 and 2695 cm^{-1} did not reveal new significant aldehyde-specific peaks, further supporting the identification of aldehydic groups at 1733 cm^{-1}.

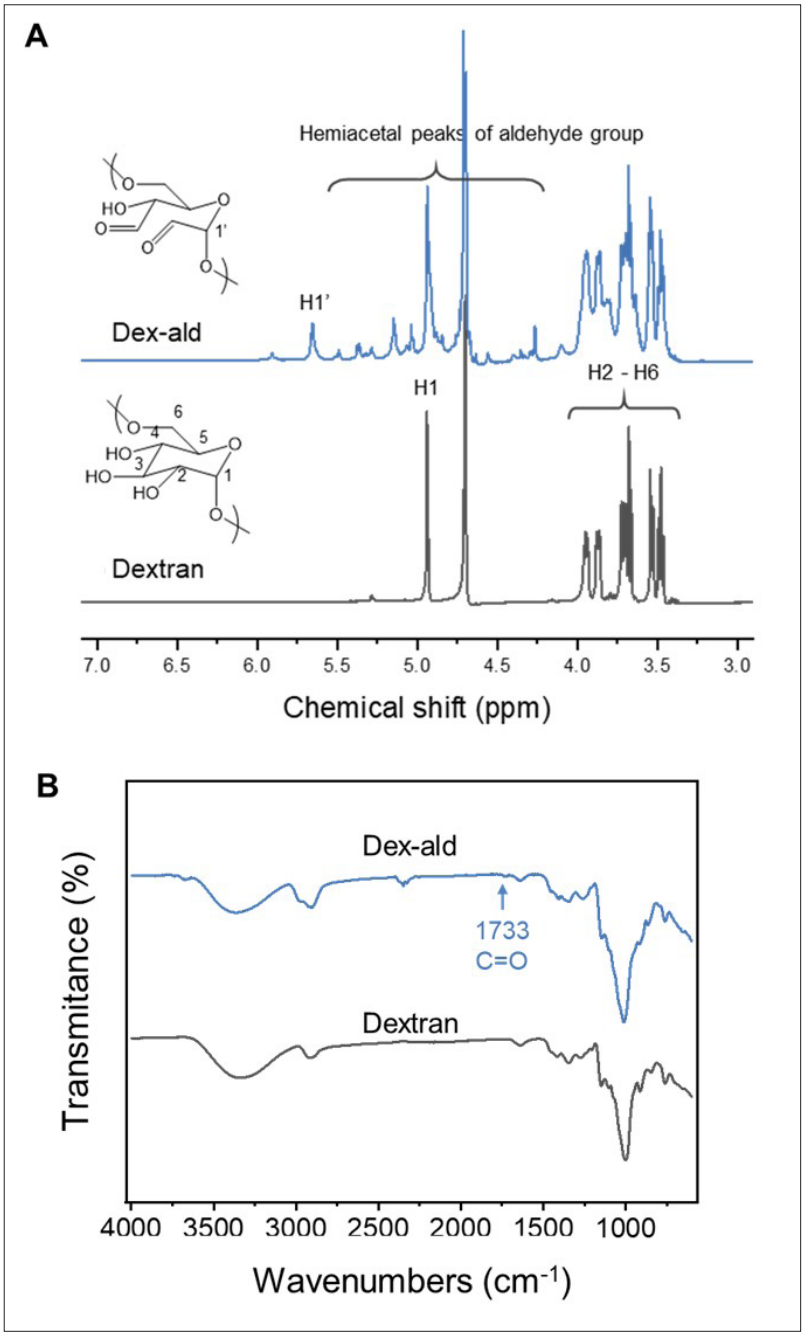

Figure 2. Characterization of dextran-aldehyde (dex-ald). (A) ^{1}H NMR spectra confirming the successful oxidation of dextran to dex-ald. (B) FTIR spectra of dextran and dex-ald showing an aldehyde-specific peak at 1733 cm^{-1}, which is indicated by an arrow. Abbreviation: FTIR, Fourier-transform infrared spectroscopy.

Figure S1A (Supporting Information in the Supplementary File) displays the FTIR spectra of the bioink components, including gelatin, alginate, dextran, and dex-ald. The presence of a peak at 1595 cm^{-1} in the gelatin spectrum indicates the amide group, which is expected to form Schiff base bonds with the aldehyde group in dex-ald. The molecular weights of alginate, gelatin, dextran, and dex-ald were 2.53 (± 0.11) × 10^5, 2.06 (± 0.05) × 10^5, 3.69 (± 0.03) × 10^5, and 4.65 (± 0.26) × 10^4 g/mol, respectively (Table S1, Supporting Information). Figure S1B, Supporting Information shows the quantification of functional groups involved in crosslinking. The aldehyde content in dextran-aldehyde (dex-ald) was determined via hydroxylamine titration,

whereas amine group quantification in gelatin was performed using TNBSA assay. AGDA1 bioink contained 3.5 mmol/g of amine functional group and 0.3 mmol/g of aldehyde functional group. The results indicate sufficient aldehyde and amine functional groups to form Schiff base crosslinking within the AGDA bioink.

3.1.2. Characterization of AGDA bioinks

The mechanical properties of AGDA bioinks with varying dex-ald concentrations (0%, 1%, 2%, and 3%) were evaluated to determine their suitability for bioprinting. Oscillatory rheology analysis of the elastic (G') and viscous (G'') moduli was performed during incubation at 4 °C for 20 min, followed by 25 °C for 20–80 min (Figure 3A). Although G' alone is not sufficient to predict printing performance, previous studies have shown that the balance between G' and viscosity is critical for achieving high print fidelity and maintaining shape integrity during extrusion. At 4 °C, all bioinks exhibited higher storage moduli (G') than loss moduli (G''), indicating that the bioinks predominantly exhibit elastic behaviors, which make them suitable for maintaining shape during printing.[33] Upon incubation at 25 °C, the G' values showed a gradual decrease, reflecting a transition to a more fluidic character at room temperature. AGDA3 displayed the highest G' throughout the experiment, followed by AGDA2, AGDA1, and AGDA0, indicating that increased dex-ald concentration enhances the mechanical stiffness of the bioink, likely due to increased Schiff-base formation within the bioink matrix.

Viscosity profiles of the bioinks were analyzed at 30 and 70 min after mixing over a shear rate range of 0.1–100 s^{-1} (Figure 3B and C). All bioinks exhibited shear-thinning behavior, as characterized by decreasing viscosity coupled with increasing shear rates, an attribute that makes them suitable for 3D printing. While alginate-containing bioinks (AGDA1, AGDA2, and AGDA3) showed similar viscosity at 1 s^{-1} initially, AGDA2 and AGDA3 displayed significant viscosity increases by 70 min, indicating progressive Schiff-base crosslinking. The shear modulus (G') of the bioinks at 1 Hz, assessed at 30 and 70 min (Figure 3E), confirmed enhanced mechanical strength and stability over time for AGDA2 and AGDA3 compared to AGDA0 and AGDA1.

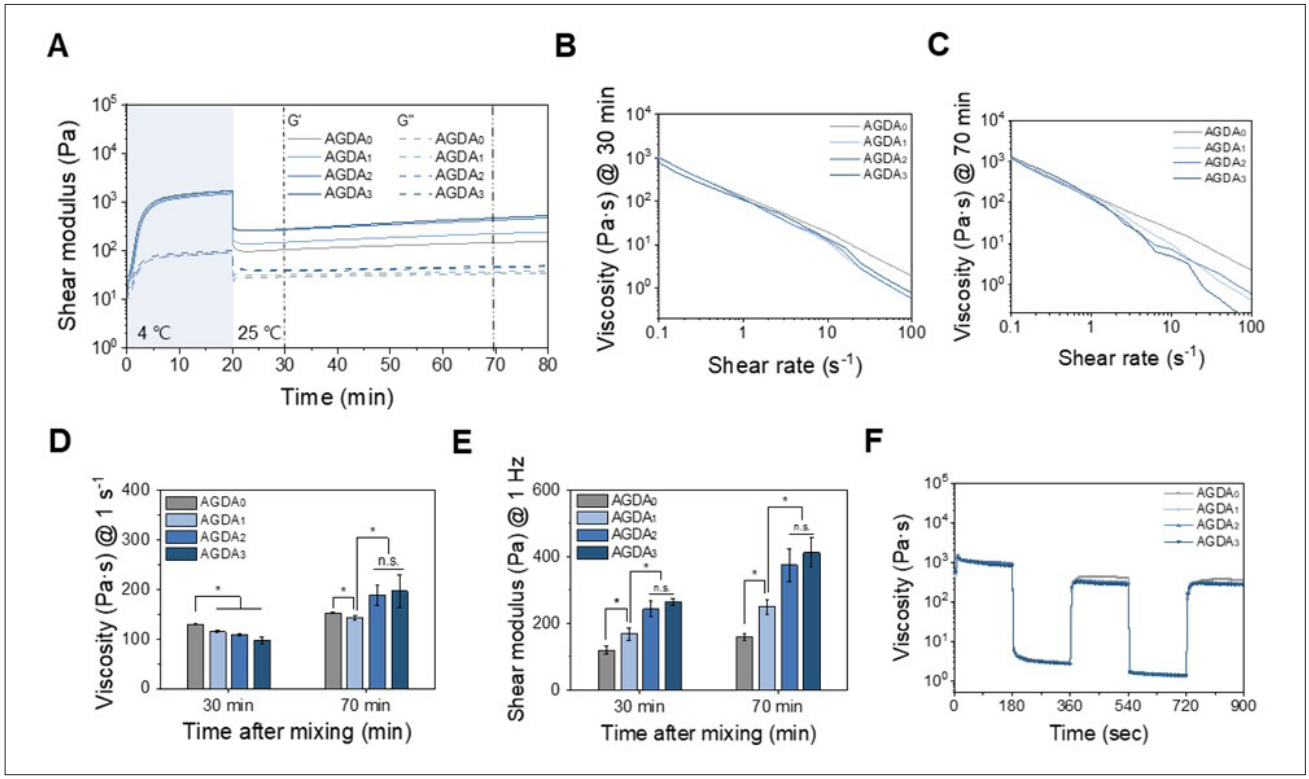

Figure 3. Rheological properties of AGDA bioinks with varying dex-ald concentrations (0%, 1%, 2%, and 3%). (A) Shear elastic (G') and viscous (G'') moduli measured during incubation at 4 °C and subsequently at 25 °C. (B, C) Viscosity profiles of bioinks at shear rates ranging from 0.1 to 100 s^{-1} at 30 and 70 min. (D) Shear modulus and (E) viscosity at a shear rate of 1 s^{-1} at 30 and 70 min. (F) Thixotropic behavior assessed by alternating shear rates of 0.1 and 50 s^{-1}. *$p < 0.05$. Abbreviations: AGDA, alginate/gelatin/dextran-aldehyde; Dex-ald, dextran-aldehyde.

Mechanical property changes after mixing were assessed by comparing shear moduli and viscosities measured at 30 and 70 min (Figure S2, Supporting Information). AGDA0 and AGDA1 showed no significant changes, whereas AGDA2 and AGDA3 exhibited notable increases in modulus and viscosity, suggesting the need for adjusted printing conditions (e.g., extrusion pressure) to maintain print fidelity.

The thixotropic properties of the bioinks were evaluated by simulating the shear forces during extrusion through a printing needle. Appropriate thixotropy, characterized by efficient viscosity recovery, ensures minimal strand spreading and high-fidelity 3D structures. Specifically, the thixotropic behavior of AGDA bioinks was assessed by measuring viscosity recovery under alternating low (0.1 s^{-1}) and high (50 s^{-1}) shear rates (Figure 3F). AGDA0, AGDA1, AGDA2, and AGDA3 demonstrated viscosity recovery rates of 43.7 ± 4.7%, 36.9 ± 7.7%, 43.3 ± 6.9%, and 28.6 ± 12.7%, respectively, indicating suitable structural resilience for bioprinting applications (Figure S3, Supporting Information).

In vitro degradation studies examined the biodegradability of AGDA bioinks by incubating them in 0.15 M NaCl with 0.1% $CaCl_2$ (Figure S4, Supporting Information). Both AGDA0 and AGDA1 showed gradual degradation, with AGDA1 degrading more slowly due to Schiff base linkages between dex-ald and gelatin, reducing the burst release of gelatin. Further testing in the absence of calcium ions (Figure S5, Supporting Information) revealed that AGDA1 completely degraded within 24 h in 0.15 M NaCl. As AGDA components are biodegradable via enzymatic and hydrolytic pathways, including reversible Schiff-base dissociation, AGDA bioinks are expected to exhibit *in vivo* biodegradability. Such biodegradability is advantageous for tissue engineering, as it allows newly regenerating tissues to integrate seamlessly with host tissues.

3.2. Cytotoxicity and biocompatibility of AGDA bioinks

The cytotoxicity and biocompatibility of AGDA bioinks were evaluated using ISO cytotoxicity protocols, with PU-ZDEC as the positive control and GelXA, a commercially available bioink, as the negative control (Figure 4A, Table 3). The PU-ZDEC group exhibited severe cytotoxicity (Grade 4) according to the toxicity criteria outlined in Table 2, characterized by significant cell death and a large zone of reactivity. Similarly, AGDA3 displayed severe cytotoxicity, with results comparable to those observed for PU-ZDEC. In contrast, AGDA1 and AGDA2 showed no visible cytotoxicity, indicating their potential suitability for cell-based applications. When skeletal muscle cells were used, a distinct pattern of biocompatibility emerged. Unlike fibroblasts, skeletal muscle cells maintained high viability even in the AGDA3 bioink.

Further, to assess the bioinks' biocompatibility in encapsulation conditions, cells were embedded within the bioinks and cultured (Figure 4B and C). Live/dead analysis, including the quantitative counting of live and dead cells, revealed a significant increase in cell death for fibroblasts encapsulated in AGDA3, particularly around areas of polymer concentration. In AGDA3, a sharp increase in dead fibroblasts was observed after encapsulation, consistent with the cytotoxicity seen in surface analysis. However, skeletal muscle cells demonstrated a stark contrast, maintaining high viability in AGDA3 bioinks during encapsulation studies. This suggests that the mechanical stiffness of AGDA3, while challenging for fibroblasts, may provide a conducive environment for skeletal muscle cells, which are known to thrive in stiffer matrices that mimic their native tissue environment.

3.3. Printability testing of AGDA bioink

Print fidelity was evaluated based on the following criteria: (1) line resolution, defined as the ratio of printed filament

Table 3. Direct contact cytotoxicity assay of bioink (n = 3)

Sample	Fibroblasts		Skeletal muscle cells	
	Formed zone size (cm)	Zone index	Formed zone size (cm)	Zone index
Non-treatment	0	0	0	0
PU-ZDEC	1.03 ± 0.13	4	0.58 ± 0.06	3
Gel-XA	0	0	0	0
$AGDA_0$	0	0	0	0
$AGDA_1$	0	0	0	0
$AGDA_2$	0	0	0	0
$AGDA_3$	1.59 ± 0.03	4	-	-

Abbreviations: AGDA, alginate/gelatin/dextran-aldehyde; PU-ZDEC, polyetherurethane film containing 0.1% zinc diethyldithiocarbamate.

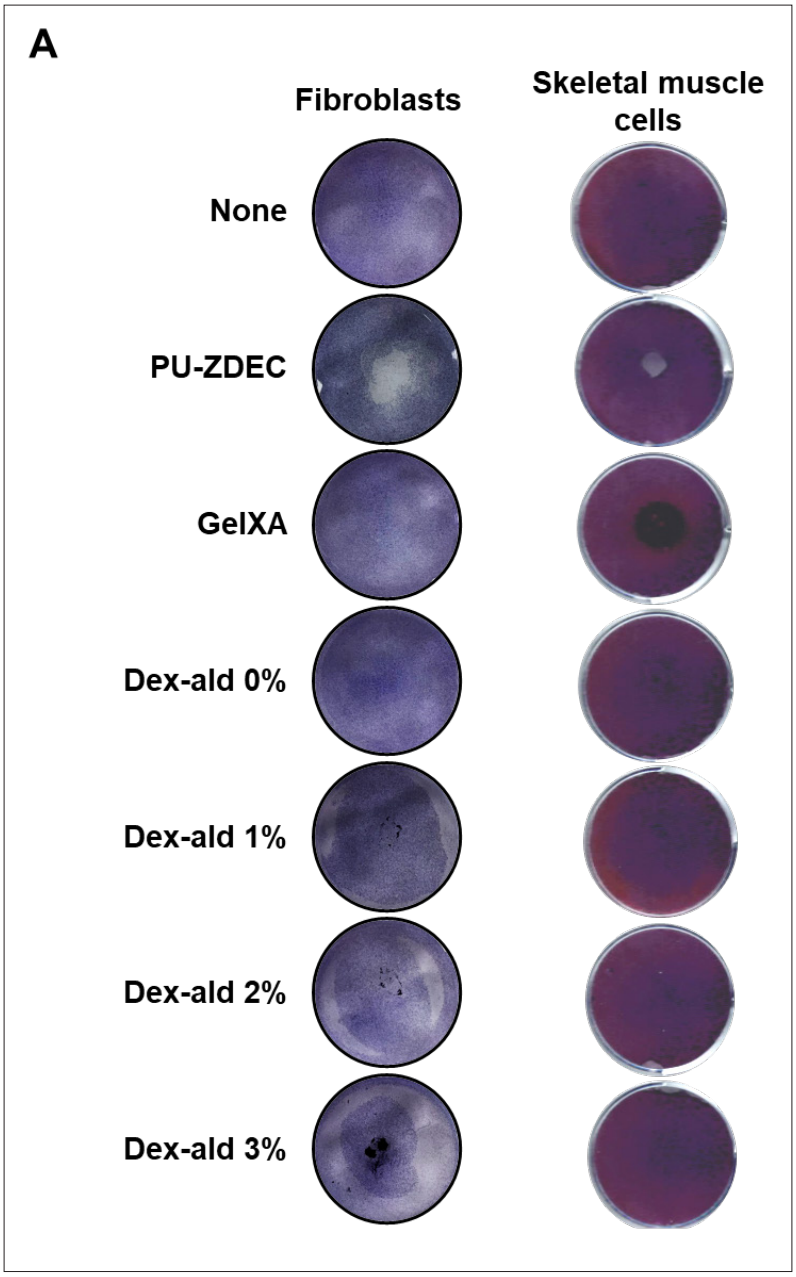
A
Fibroblasts
Skeletal muscle cells
None
PU-ZDEC
GelXA
Dex-ald 0%
Dex-ald 1%
Dex-ald 2%
Dex-ald 3%

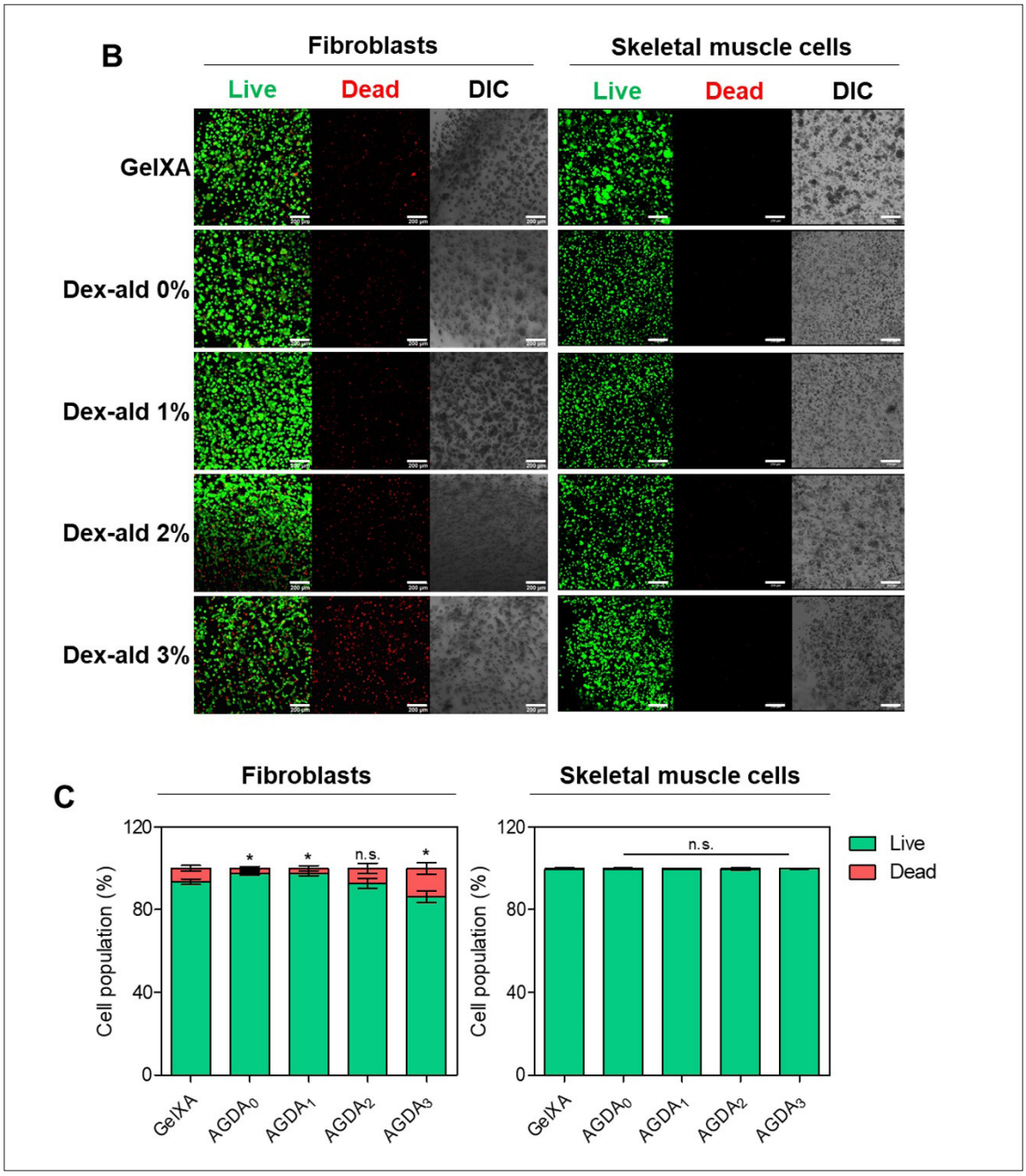

Figure 4. Cytotoxicity evaluation of AGDA bioinks. (A) Hematoxylin staining of fibroblasts and skeletal muscle cells for comparison of cytotoxicity zones between AGDA1, AGDA2, AGDA3, and PU-ZDEC (positive control). (B) Live/Dead staining results of fibroblasts and skeletal muscle cells encapsulated within AGDA bioinks at day 3. Scale bars: 200 μm. (C) Graph of quantitative results of counting live and dead cells respectively. Abbreviations: AGDA, alginate/gelatin/dextran-aldehyde; Dex-ald, dextran-aldehyde; DIC, differential interference contrast ___; PU-ZDEC, polyetherurethane film containing 0.1% zinc diethyldithiocarbamate.

width to nozzle diameter, ensuring minimal deviation; (2) shape fidelity, which refers to the geometric accuracy of printed structures compared to the digital model; and (3) structural stability, representing the retention of printed constructs without significant deformation post-printing.[34–36] Printing pressure, speed, nozzle diameter, and the distance between the printing nozzle and the substrate are essential parameters for optimizing the bioprinting process, and it is crucial to fine-tune these parameters based on the type of bioink used.[34] Excessively high pressure results in excessive bioink extrusion, reducing printability, whereas excessively high speed may cause the extruded bioink to break, leading to lower print fidelity.[35] Additionally, if there is a huge distance between the printing nozzle and the substrate, the extruded bioink width may decrease, potentially improving resolution but increasing the risk of discontinuous extrusion.[36] Therefore, process parameter optimization is essential for achieving optimal printability.

To identify the optimal conditions for 3D bioprinting of AGDA1 bioink, we systematically varied the pneumatic pressure (120–280 kPa) and printing speed (600–1600 mm/min) while maintaining a constant nozzle diameter (22 G). This allowed us to assess the effect of these parameters on print quality criteria such as strand continuity, line resolution, and construct stability. The selected bioink's rheological profile, in conjunction with process parameters, guided our optimization for both acellular and cell-laden formulations. A printability map was constructed based on these parameters to identify the ideal combination of pressure and speed for achieving high printing quality and efficiency (Figure 5A and C). In the printability map, the gray X symbols denote instances of printing line breakage or merging, while the yellow triangle symbols indicate scenarios where lines persist yet lack coherence due to suboptimal printability. The blue circle and double circle marks present conditions of high printability, with the double circle marks denoting the conditions used in the experiments. As shown in the printability map (Figure 5), low pressures (<160 kPa) at high printing speeds led to filament discontinuity due to insufficient extrusion, whereas high pressures (>240 kPa) resulted in excessive material flow and loss of structural resolution. These observations emphasize the need to fine-tune pressure and speed combinations to achieve balanced extrusion and high-fidelity constructs, as supported by previous studies on alginate-based inks.[37] For the acellular AGDA1 bioink, the optimal parameters were determined to be a 22G nozzle, a pressure of 240 kPa and a printing speed of 1200 mm/min, producing smooth, continuous lines with excellent fidelity. In the cell-laden AGDA1 bioink, the presence of cells slightly altered the flow behavior, requiring a reduced pressure of 160 kPa while maintaining the same printing speed of 1200 mm/min to prevent cellular damage and ensure uniform extrusion. These optimized parameters not only enhanced printing accuracy but also shortened the printing time, making them suitable for fabricating large-scale structures.

The printability of AGDA1 bioink was further assessed by creating three distinct 3D patterns: a serpentine structure with a 5 mm gap, and square and reticular structures with single and double layers (10 × 10 mm^2) (Figure 5B and D). The printed constructs closely matched the intended design, demonstrating high fidelity in both acellular and cell-laden conditions. The bioink tracks remained uninterrupted, with each line distributed independently without merging or collapsing. This high shape fidelity is critical for preserving the microporosity of the constructs, facilitating the transfer of oxygen, nutrients, and metabolic waste necessary for tissue viability and function. These results confirm that AGDA1 bioink can achieve consistent and precise printing performance under optimized conditions, supporting its applicability for fabricating complex and scalable 3D tissue constructs in both acellular and cell-laden formats.

3.4. Fabrication and characterization of fibroblast spheroids for encapsulation

To identify the optimal conditions for cell engraftment and tissue regeneration using AGDA1 bioink, fibroblasts were encapsulated in the following three formats: single cells, spheroids, and a combination of single cells and spheroids. As a prerequisite, fibroblast spheroids were fabricated using a mesh-integrated ULA dish, as illustrated in Figure 6A. The ULA dish enabled uniform cell distribution and facilitated efficient spheroid formation.

The spheroid fabrication process is shown in Figure 6B. Upon plating fibroblasts onto the ULA dish, the cells were evenly distributed across the surface. By day 1, fibroblasts had aggregated successfully to form spheroids. These spheroids maintained their compact and uniform structure throughout the 7-day culture period, demonstrating stability and reproducibility. The average diameter of the spheroids was initially approximately 120 μm and decreased slightly over the culture period, reaching 100 μm by day 7 (Figure 6C). This minor size reduction is likely attributed to increased cell–cell adhesion over time, which strengthens the structural integrity of the spheroids.

To evaluate the viability of the spheroids before encapsulation, Live/Dead staining was performed on day 7 (Figure 6D). The results showed that the majority of cells within the spheroids remained viable, with minimal cell death observed. The high cell viability further highlights

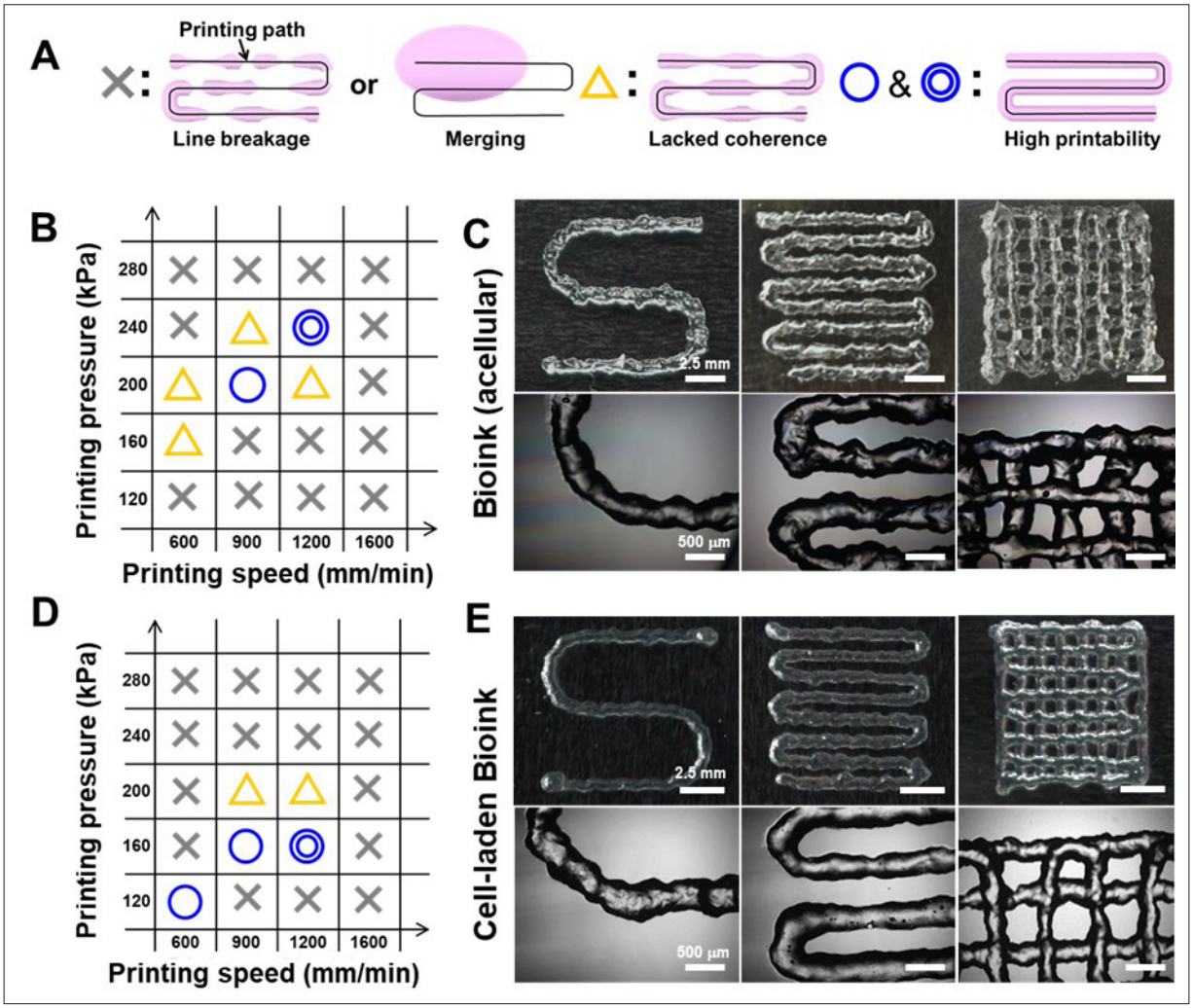

Figure 5. Printability assessment of AGDA1 bioink. (A) Graphical annotations to indicate key printability criteria (X, triangle, and circle symbols). (B, C) Acellular AGDA1 bioink printed under optimized conditions with a pressure of 240 kPa and a speed of 1200 mm/min. (D, E) Cell-laden AGDA1 bioink printed with a reduced pressure of 160 kPa and the same speed. The symbols in the printability map (B and D) were designed to represent the different levels of printability observed under various experimental conditions. The gray X symbols indicate conditions where printing resulted in line breakage or merging, representing low printability; the yellow triangle symbols denote scenarios where the printed lines were present but lacked coherence due to suboptimal printability; the blue circle symbols represent conditions with high printability, characterized by well-defined, coherent lines; the blue double circle symbols highlight the specific conditions used in our experiments, signifying the optimal settings that achieved both high print fidelity and cell compatibility. Abbreviation: AGDA, alginate/gelatin/dextran-aldehyde.

the stability and robustness of the spheroids, ensuring their suitability for encapsulation experiments.

These results demonstrate the successful fabrication of fibroblast spheroids with uniform size, high viability, and excellent structural stability. The slight reduction in spheroid size during the culture period is likely due to enhanced cell–cell adhesion, which contributes to the compact and cohesive nature of the spheroids. These high-quality spheroids, along with single cells and mixed formats, were used in subsequent experiments to assess the optimal conditions for cell encapsulation and engraftment in AGDA1 bioink.

3.5. Cell survival and morphological changes in AGDA1 bioink

The long-term survival and engraftment of fibroblasts encapsulated in AGDA1 bioink were evaluated using the following three encapsulation methods: single cells, spheroids, and a combination of both. Commercially available GelXA bioink served as the control. The encapsulated cells were cultured for 14 days, and observations were made on days 1, 7, and 14 to assess cell

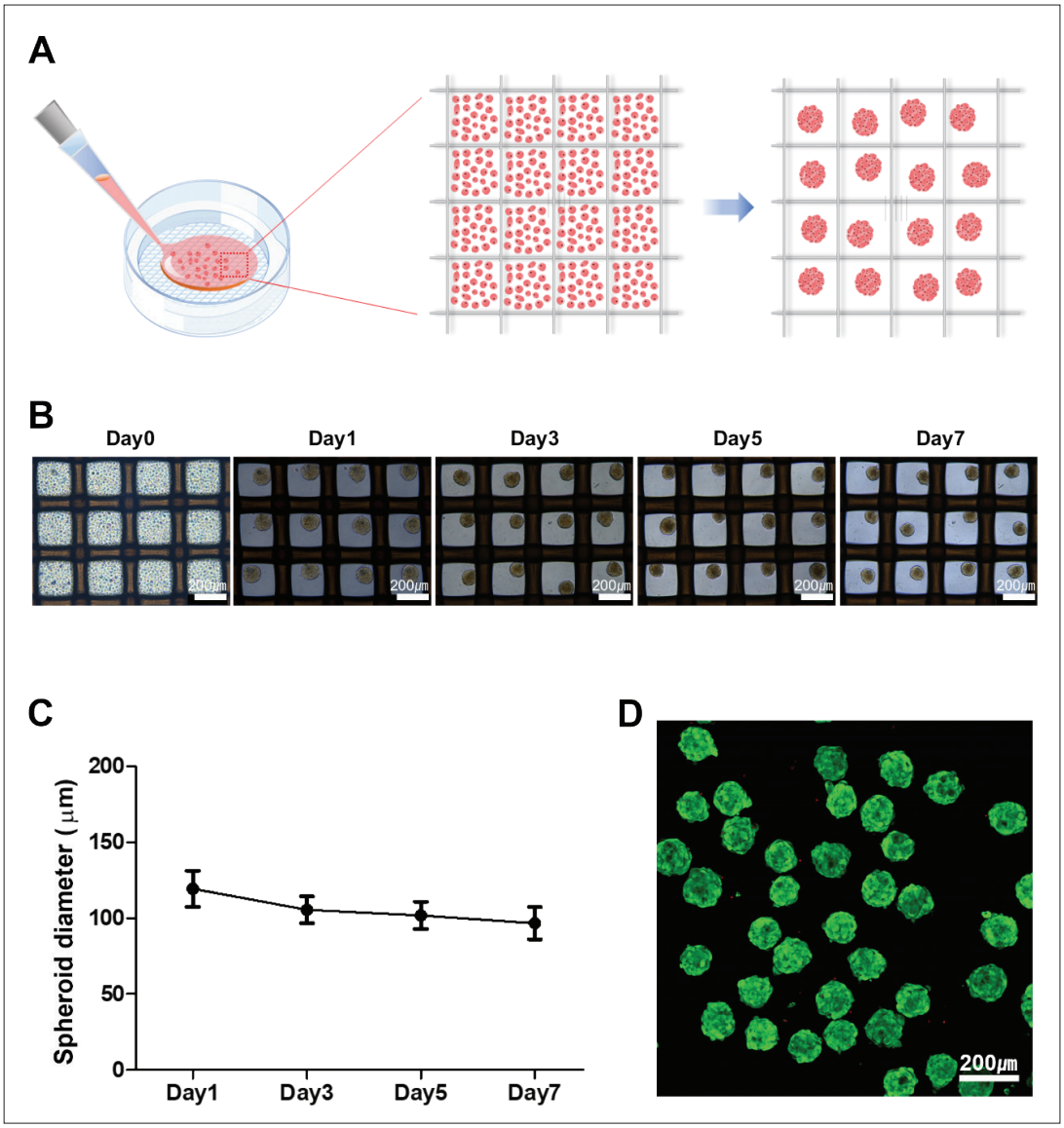

Figure 6. Fabrication and characterization of fibroblast spheroids. (A) Schematic of spheroid preparation using ultra-low attachment (ULA) culture dishes. (B) Optical images showing spheroid formation on day 1, with uniform size and morphology maintained over 7 days. Scale bars: 200μm. (C) Quantitative analysis of spheroid size, demonstrating a slight reduction in size due to enhanced cell-cell adhesion. (D) Live/Dead staining on day 7 confirming high viability of spheroid cells prior to encapsulation.

survival, morphology, and cellular density (Figure 7A–C). On day 1, Live/Dead staining revealed high cell viability across all groups, with minimal cell death observed regardless of the bioink type or encapsulation method. Over the course of 14 days, significant differences in cell morphology and behavior were noted between the GelXA and AGDA1 groups. Cells encapsulated in GelXA maintained their original round shape throughout the culture period, with little to no morphological changes observed. In contrast, cells in AGDA1 bioink began to adopt fibroblast-like spindle shapes by day 7, a characteristic indicative of active spreading and functional engagement with the surrounding matrix. By day 14, fibroblasts in AGDA1 bioink exhibited a highly elongated morphology, accompanied by a noticeable increase in cellular density.

Quantitative analysis of cellular density (Figure 7D) confirmed that AGDA1 bioink supported greater cell proliferation compared to GelXA. Among the AGDA1 groups, the combination of single cells and spheroids resulted in the highest cellular density, surpassing that

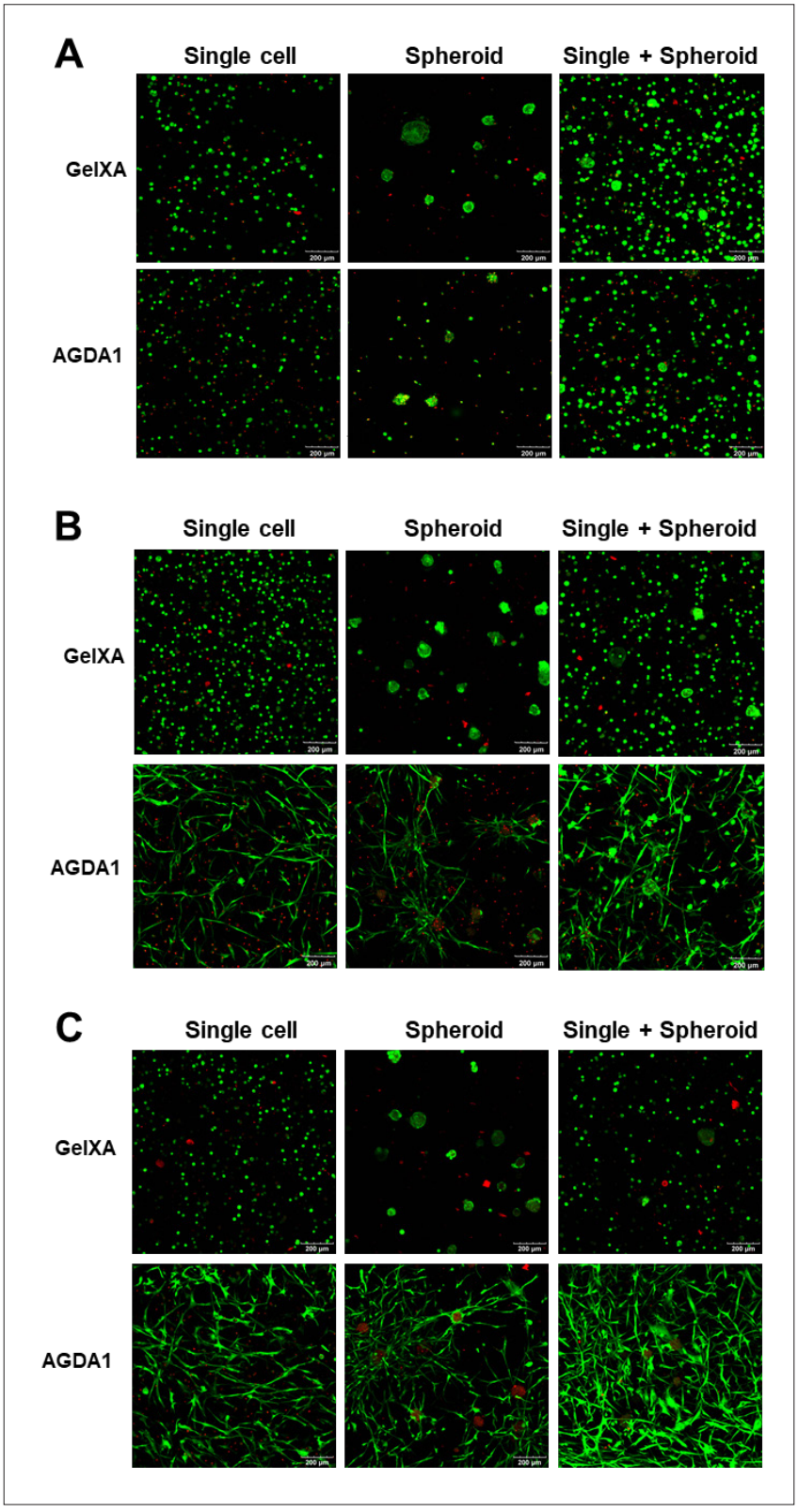
A
Single cell
Spheroid
Single + Spheroid
GelXA
AGDA1
B
Single cell
Spheroid
Single + Spheroid
GelXA
AGDA1
C
Single cell
Spheroid
Single + Spheroid
GelXA
AGDA1

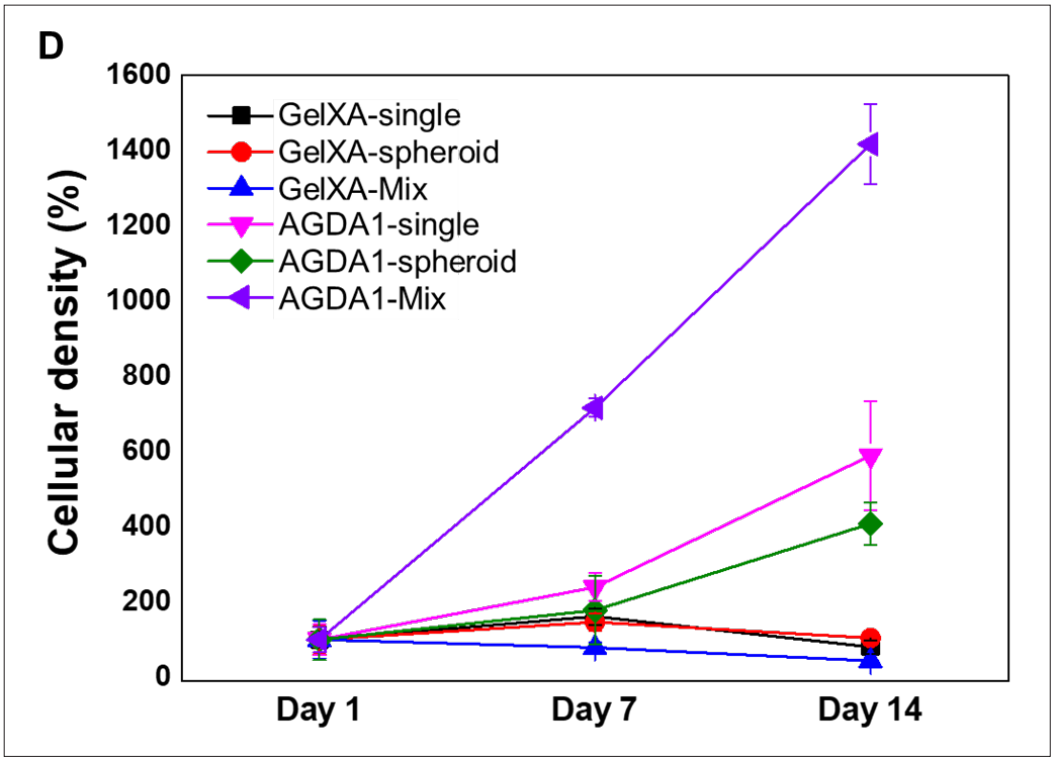

Figure 7. Cell survival and morphological changes in AGDA1 bioink. (A–C) Live/Dead staining images of fibroblasts encapsulated in AGDA1 bioink as single cells, spheroids, or a combination, compared to the GelXA control, on days 1, 7, and 14. Scale bars: 200μm. (D) Quantitative analysis of cellular density shows significantly higher cell proliferation in AGDA1 compared to GelXA, with the combination method demonstrating the highest density. By day 14, fibroblasts in AGDA1 exhibited spindle-like morphology, indicating active matrix engagement and functional behavior. Abbreviation: AGDA, alginate/gelatin/dextran-aldehyde.

of the single-cell or spheroid-only groups. This suggests that the combination method provides an optimal microenvironment, balancing cell–cell interactions from spheroids with the uniform distribution of single cells, thereby promoting enhanced engraftment and proliferation.

These results demonstrate that AGDA1 bioink provides a superior environment for fibroblast survival, morphological transformation, and proliferation compared to the commercially available GelXA bioink. The enhanced cellular density and fibroblast-like morphology in AGDA1 suggest its potential to support tissue regeneration and functionality over prolonged culture periods.

4. Discussion

In this study, we developed and characterized a novel AGDA bioink optimized for printability, mechanical properties, and biocompatibility, aiming to enhance tissue regeneration. Our results demonstrated that AGDA1, with its balanced composition of alginate, gelatin, and dex-ald, outperformed other formulations and the commercially available GelXA bioink in supporting cell survival, proliferation, and morphological transformation. These findings not only highlight AGDA1's potential for bioprinting but also provide valuable insights into the relationship between bioink composition, mechanical properties, and cellular behavior.

The performance of AGDA bioink is largely attributed to the complementary roles of its components. Alginate, a natural polysaccharide derived from brown algae, provides the backbone for the bioink's structural integrity.[38] The gelation of alginate is achieved through ionic crosslinking with calcium ions, which provides rapid gelation and structural integrity.[9–12] This process is crucial in maintaining the shape of bioprinted structures. Unlike photocrosslinked bioinks such as GelXA, which require additional curing steps, alginate-calcium gelation occurs immediately upon exposure to Ca^{2+}, contributing to improved printability and post-printing stability. However, alginate alone lacks bioactive sites for cell adhesion and interaction, necessitating the inclusion of additional components to improve biocompatibility. Dextran-aldehyde (dex-ald)

was incorporated as a chemical crosslinker to enhance the mechanical properties and tunability of the bioink. The aldehyde groups of dex-ald form Schiff base linkages with the amino groups of gelatin, creating a chemically crosslinked network that complements the physical gelation of alginate.[9–12] This dual-crosslinking strategy not only strengthens the bioink matrix but also allows for tunable stiffness by varying the concentration of dex-ald, as observed in the superior mechanical properties of AGDA3. Gelatin, a collagen-derived protein, plays a critical role in improving cell compatibility by providing bioactive sites for cell adhesion, proliferation, and differentiation.[39–41] Its thermosensitive properties also contribute to the gelation process, enhancing the overall stability of the bioink at physiological temperatures.[11] Furthermore, gelatin's interaction with dex-ald enhances the cohesiveness of the hydrogel network, ensuring that encapsulated cells remain embedded and supported during bioprinting and culture.[39]

The mechanical performance of AGDA bioinks, particularly AGDA1, was enhanced through a dual-crosslinking strategy combining ionic gelation of alginate with Schiff base formation between dex-ald and gelatin. This approach aligns with established principles that hybrid crosslinking methods contribute to mechanical tunability and stability in hydrogel-based bioinks.[15–17] The superior print fidelity of AGDA1 can be attributed to its optimal rheological profile, which balances viscosity and elasticity to support both extrusion and post-printing stability. The effective printability of AGDA1 bioink may also benefit from intrinsic pre-crosslinking behavior arising from partial Schiff base interactions occurring shortly after mixing, which increase the bioink's viscosity before extrusion. Such pre-crosslinking behavior has been shown in a previous study[42] to enhance the structural stability of bioinks during deposition by supporting strand formation and reducing spreading. As shown in Figure 5, AGDA1 demonstrated a good print fidelity under optimized conditions. This high fidelity is attributed to a balanced viscoelastic property, with an appropriate storage modulus (G') supporting shape retention and a high viscosity recovery rate enabling structural stability after extrusion. Comparable studies have shown that bioinks with similar G' values (ranging from 800 to 1500 Pa) exhibit high printing accuracy and structural integrity, further supporting the suitability of AGDA1 for bioprinting applications.[33,43] Our findings also highlight the importance of tailoring bioink compositions to match specific bioprinting requirements. While AGDA3 exhibited the highest mechanical stiffness, its increased viscosity led to cytotoxic effects for fibroblasts. However, it was not toxic to skeletal muscle cells. This highlights the need to optimize bioink formulations to maintain cell compatibility, as different organ-forming cells have different preferred physical properties. This balance between mechanical properties and biocompatibility is well-documented in the literature, where overly stiff hydrogels often impede cell proliferation and migration.[44–46] The printability map generated in this study provides a valuable tool for identifying the optimal printing parameters for AGDA bioinks, facilitating reproducible and high-quality 3D-printed constructs. Furthermore, the specific roles of each bioink component are critical in achieving the dual objectives of printability and cell compatibility. Alginate provides rapid ionic gelation, contributing to structural stability and print fidelity. Gelatin offers bioactive motifs for cell attachment, enhancing biocompatibility and promoting cell adhesion, proliferation, and differentiation. Dextran-aldehyde introduces mechanical tunability through Schiff base formation, allowing for adjustable stiffness and maintaining cell-friendly conditions at optimized concentrations. The synergistic effect of these components ensures that AGDA1 not only supports cellular health but also maintains the architectural integrity of printed structures.

When fibroblasts were encapsulated in AGDA1 using single cells, spheroids, or a combination of both, notable differences in cellular behavior emerged. AGDA1 supported fibroblast survival across all conditions, but its ability to facilitate morphological transformation and proliferation was particularly striking. Unlike GelXA, which maintained cells in their rounded shapes throughout the culture period, AGDA1 enabled fibroblasts to adopt their characteristic spindle-like morphology, indicative of active interaction with the bioink matrix. Furthermore, quantitative analysis of cellular density revealed that the combination of single cells and spheroids yielded the highest proliferation rate, suggesting that this method creates a synergistic microenvironment by combining the advantages of cell–cell interactions within spheroids and the uniform distribution of single cells.

These findings align with prior studies, emphasizing the importance of bioink composition and encapsulation strategies in tissue regeneration. Our results demonstrated that AGDA1 bioink supported survival rates of fibroblasts and skeletal muscle cells, which were similar to that observed with GelXA (Figure 4). The combination encapsulation method facilitated enhanced cellular density (Figure 7D), with a 1.8-fold increase over single-cell encapsulation. This is consistent with previous studies indicating that bioinks incorporating both single cells and spheroids can promote more efficient tissue regeneration due to enhanced cell–cell interactions.[44] Furthermore, AGDA1 bioink exhibited biodegradability essential for tissue regeneration under physiological conditions (Figure S4, Supporting Information).[47] However, our dual-crosslinking approach,

leveraging both ionic gelation and Schiff base formation, offers a more refined balance of mechanical properties and biocompatibility compared to conventional bioinks. This study advances the field by demonstrating that AGDA1 is capable of addressing critical limitations seen in both overly stiff and overly compliant bioinks, providing a versatile platform for diverse bioprinting applications.

Despite these promising results, there are limitations to address. For instance, the long-term *in vivo* performance of AGDA1 bioink and its degradation profile remain unexplored. Future studies should focus on evaluating AGDA1's capacity to support vascularization, immune compatibility, and integration with host tissues in animal models. Additionally, the combination encapsulation approach warrants further investigation to optimize the ratio of single cells to spheroids for specific tissue types, potentially tailoring AGDA1 for applications such as skin, cartilage, or vascular tissues.

5. Conclusion

The findings of this study demonstrate that AGDA1 bioink offers a balance between mechanical stability, biocompatibility, and printability, making it a promising candidate for regenerative medicine applications. Future research should focus on validating AGDA1 bioink in *in vivo* models to assess long-term biocompatibility and functional tissue regeneration.

Acknowledgments

None.

Funding

This research was supported by the Challengeable Future Defense Technology Research and Development Program through the Agency For Defense Development (ADD) funded by the Defense Acquisition Program Administration (DAPA) in 2024 (No. 915060201).

Conflict of interest

The authors declare they have no competing interests.

Author contributions

Conceptualization: Jae Young Lee, Junhee Lee, Sun-Woong Kang
Data curation: Hosub Lim, Daun Seo
Formal analysis: Kyung Deok Park, Hye-Eun Shim, Ji Hye Park, Eun-Jung Ann
Funding acquisition: Junhee Lee
Methodology: Hosub Lim, Daun Seo, Junghyun Kim
Supervision: Jae Young Lee, Junhee Lee, Sun-Woong Kang
Writing–original draft: Jae Young Lee, Sun-Woong Kang
Writing–review & editing: Sun-Woong Kang

Ethics approval and consent to participate

Not applicable.

Consent for publication

Not applicable.

Availability of data

All data generated and/or analyzed during this study are included in this published article.

References

1. Dey M, Ozbolat IT. 3D bioprinting of cells, tissues and organs. *Sci Rep*. 2020;10(1):14023. doi: 10.1038/s41598-020-70086-y2
2. Shukla P, Yeleswarapu S, Heinrich MA, Prakash J, Pati F. Mimicking tumor microenvironment by 3D bioprinting: 3D cancer modeling. *Biofabrication*. 2022;14(3):032002. doi: 10.1088/1758-5090/ac6d11
3. Wang Z, Xiang L, Lin F, Tang Y, Cui WJ. 3D bioprinting of emulating homeostasis regulation for regenerative medicine applications. *Control Release*. 2023;353:147-165. doi: 10.1016/j.jconrel.2022.11.035
4. Maharjan S, Ma C, Singh B, et al. Advanced 3D imaging and organoid bioprinting for biomedical research and therapeutic applications. *Adv Drug Deliv Rev*. 2024;208:115237. doi: 10.1016/j.addr.2024.115237
5. Zennifer A, Manivannan S, Sethuraman S, Kumbar SG, Sundaramurthi D. 3D bioprinting and photocrosslinking: emerging strategies & future perspectives. *Biomater Adv*. 2022;134:112576. doi: 10.1016/j.msec.2021.112576
6. Zhang J, Wehrle E, Rubert M, Müller R. 3D bioprinting of human tissues: biofabrication, bioinks, and bioreactors. *Int J Mol Sci*. 2021;22(8):3971. doi: 10.3390/ijms22083971
7. Zhang W, Kuss M, Yan Y, Shi W. Dynamic alginate hydrogel as an antioxidative bioink for bioprinting. *Gels*. 2023;9(4):312. doi: 10.3390/gels9040312
8. Lan X, Ma Z, Szojka ARA, et al. TEMPO-oxidized cellulose nanofiber-alginate hydrogel as a bioink for human meniscus tissue engineering. *Front Bioeng Biotechnol*. 2021;9:766399. doi: 10.3389/fbioe.2021.766399
9. Kim J, Choi YJ, Gal CW, Sung A, Park H, Yun HS. Development of an alginate-gelatin bioink enhancing osteogenic differentiation by gelatin release. *Int J Bioprint*. 2023;9(2):660. doi: 10.18063/ijb.v9i2.660

10. Gao Q, Kim BS, Gao G. Advanced strategies for 3D bioprinting of tissue and organ analogs using alginate hydrogel bioinks. *Mar Drugs*. 2021;19(12):708. doi: 10.3390/md19120708

11. Hao L, Zhao S, Hao S, et al. Functionalized gelatin-alginate based bioink with enhanced manufacturability and biomimicry for accelerating wound healing. *Int J Biol Macromol*. 2023;240:124364. doi: 10.1016/j.ijbiomac.2023.124364

12. Stola GP, Paoletti C, Nicoletti L, et al. Internally-crosslinked alginate dialdehyde/alginate/gelatin-based hydrogels as bioinks for prospective cardiac tissue engineering applications. *Int J Bioprint*. 2024:10;4014. doi: 10.36922/ijb.4014

13. Cruz EM, Machado LS, Zamproni LN, et al. A gelatin methacrylate-based hydrogel as a potential bioink for 3D bioprinting and neuronal differentiation. *Pharmaceutics*. 2023;15(2):627. doi: 10.3390/pharmaceutics15020627

14. Shi W, Fang F, Kong Y, et al. Dynamic hyaluronic acid hydrogel with covalent linked gelatin as an anti-oxidative bioink for cartilage tissue engineering. *Biofabrication*. 2021;14(1). doi: 10.1088/1758-5090/ac42de

15. Musilová L, Achbergerová E, Vítková L, et al. Cross-linked gelatine by modified dextran as a potential bioink prepared by a simple and non-toxic process. *Polymers (Basel)*. 2022;14(3):391. doi: 10.3390/polym14030391

16. Banigo AT, Nauta L, Zoetebier B, Karperien M. Coaxial bioprinting of enzymatically crosslinkable hyaluronic acid-tyramine bioinks for tissue regeneration. *Polymers (Basel)*. 2024;16(17):2470. doi: 10.3390/polym16172470

17. Ouyang L, Armstrong JPK, Lin Y, et al. Expanding and optimizing 3D bioprinting capabilities using complementary network bioinks. *Sci Adv*. 2020;6(38):eabc5529. doi: 10.1126/sciadv.abc5529

18. Hauptstein J, Forster L, Nadernezhad A, et al. Bioink platform utilizing dual-stage crosslinking of hyaluronic acid tailored for chondrogenic differentiation of mesenchymal stromal cells. *Macromol Biosci*. 2022;22:e2100331. doi: 10.1002/mabi.202100331

19. Hu T, Cui X, Zhu M, et al. 3D-printable supramolecular hydrogels with shear-thinning property: fabricating strength tunable bioink via dual crosslinking. *Bioact Mater*. 2020;5:808-818. doi: 10.1016/j.bioactmat.2020.06.001

20. Shin JY, Yeo YH, Jeong JE, Park SA, Park WH. Dual-crosslinked methylcellulose hydrogels for 3D bioprinting applications. *Carbohydr Polym*. 2020;238:116192. doi: 10.1016/j.carbpol.2020.116192

21. Glaeser JD, Bao X, Kaneda G, et al. iPSC-neural crest derived cells embedded in 3D printable bio-ink promote cranial bone defect repair. *Sci Rep*. 2022;12:18701. doi: 10.1038/s41598-022-22502-8

22. Oliveros AL, Kingham PJ, Lammi MJ, Wiberg M, Kelk P. Three-dimensional osteogenic differentiation of bone marrow mesenchymal stem cells promotes matrix metallopeptidase 13 (MMP13) expression in Type I collagen hydrogels. *Int J Mol Sci*. 2021;22:13594. doi: 10.3390/ijms222413594

23. Chang HK, Yang DH, Ha MY, et al. 3D printing of cell-laden visible light curable glycol chitosan bioink for bone tissue engineering. *Carbohydr Polym*. 2022;287:119328. doi: 10.1016/j.carbpol.2022.119328

24. Fang Y, Ji M, Yang Y, et al. 3D printing of vascularized hepatic tissues with a high cell density and heterogeneous microenvironment. *Biofabrication*. 2023;15(4). doi: 10.1088/1758-5090/ace5e0

25. Kripamol R, Velayudhan S, Anil Kumar PR. Evaluation of allylated gelatin as a bioink supporting spontaneous spheroid formation of HepG2 cells. *Int J Biol Macromol*. 2024;274(Pt 1):133259. doi: 10.1016/j.ijbiomac.2024.133259

26. Lee HW, Chen KT, Li YE, Yeh YC, Chiang CY, Lee IC. Dual crosslinking silk fibroin/pectin-based bioink development and the application on neural stem/progenitor cells spheroid laden 3D bioprinting. *Int J Biol Macromol*. 2024; 269(Pt 2):131720. doi: 10.1016/j.ijbiomac.2024.131720

27. Sun W, Zhang J, Qin Y, et al. A simple and efficient strategy for preparing a cell-spheroid-based bioink. *Adv Healthc Mater*. 2022;11(15):e2200648. doi: 10.1002/adhm.202200648

28. Jeong JE, Han SS, Shin HE, et al. Hyaluronic microparticle-based biomimetic artificial neighbors of cells for three-dimensional cell culture. *Carbohydrate Polym*. 2022;294:119770. doi: 10.1016/j.carbpol.2022.119770

29. Schmidt SK, Schmid R, Arkudas A, Kengelbach-Weigand A, Bosserhoff AK. Tumor cells develop defined cellular phenotypes after 3D-bioprinting in different bioinks. *Cells*. 2019;8:1295. doi: 10.3390/cells8101295

30. Zhang Y, Ding Z, Liu Y, Zhang Y, Jiang S. White-light-emitting hydrogels with self-healing properties and adjustable emission colors. *J Colloid Interface Sci*. 2021;582:825-835. doi: 10.1016/j.jcis.2020.08.080

31. Kang SW, Jeon O, Kim BS. Poly(lactic-co-glycolic acid) microspheres as an injectable scaffold for cartilage tissue engineering. *Tissue Eng*. 2005;11:438-447. doi: 10.1089/ten.2005.11.438

32. Park KH, Ryu B, Song JJ, et al. Hyaluronic acid microparticles for effective spheroid culture and transplantation in liver tissue. *Chem Eng J*. 2023;464:142666. doi: 10.1016/j.cej.2023.142666

33. Im S, Choe G, Seok JM, et al. An osteogenic bioink composed of alginate, cellulose nanofibrils, and polydopamine nanoparticles for 3D bioprinting and bone tissue engineering. *Int J Biol Macromol*. 2022:205:520-529. doi: 10.1016/j.ijbiomac.2022.02.012

34. Rashik C, Muhire BS, Vijayavenkataraman S. Computational fluid dynamics assessment of the effect of bioprinting parameters in extrusion bioprinting. *Int J Bioprint* 2022;8:545. doi: 10.18063/ijb.v8i2.545

35. Andreas B, Filipa D, Campos D, et al. Controlling shear stress in 3D bioprinting is a key factor to balance printing resolution and stem cell integrity. *Adv Healthc Mater.* 2016;5:326-333. doi: 10.1002/adhm.201500677

36. Rajabi M, McConnell M, Cabral J, Ali MA. Chitosan hydrogels in 3D printing for biomedical applications. *Carbohydr Polym*. 2021;260:117768. doi: 10.1016/j.carbpol.2021.117768

37. Falcone G, Schrüfer S, Kuth S, et al. Ready-to-print alginate inks: the effect of different divalent cations on physico-chemical properties of 3D printable alginate hydrogels. *Carbohydr Polym Technol Appl.* 2024;7:100524. doi: 10.1016/j.carpta.2024.100524

38. Piras CC, Smith DK. Multicomponent polysaccharide alginate-based bioinks. *J Mater Chem B*. 2020;8(36):8171-8188. doi: 10.1039/D0TB01005G

39. Lee M, Kim YS, Park J, et al. A paintable and adhesive hydrogel cardiac patch with sustained release of ANGPTL4 for infarcted heart repair. *Bioact Mater*. 2023;31:395-407. doi: 10.1016/j.bioactmat.2023.08.020

40. Hong SJ, Kim DH, Ryoo JH, et al. Influence of gelatin on adhesion, proliferation, and adipogenic differentiation of adipose tissue-derived stem cells cultured on soy protein-agarose scaffolds. *Foods*. 2024;13(14):2247. doi: 10.3390/foods13142247

41. Li K, Wang X, Li J, Wang J, Yu W, Ge L. Bioinspired gelatin nano-film implanted into composite scaffold exhibiting both expandable adhesion and enhanced proliferation. *Int J Biol Macromol.* 2022;220:1570-1578. doi: 10.1016/j.ijbiomac.2022.09.080

42. Nelson C, Tuladhar S, Launen L, Habib MA. 3D bio-printability of hybrid pre-crosslinked hydrogels. *Int J Mol Sci*. 2021;22:13481. doi: 10.3390/ijms222413481

43. Choe G, Lee M, Oh S, et al. Three-dimensional bioprinting of mesenchymal stem cells using an osteoinductive bioink containing alginate and BMP-2-loaded PLGA nanoparticles for bone tissue engineering. *Biomater Adv*. 2022;136:212789. doi: 10.1016/j.bioadv.2022.212789

44. Kumar A, Nune KC, Murr LE, Misra RDK. Biocompatibility and mechanical behaviour of three-dimensional scaffolds for biomedical devices: process–structure–property paradigm. *Int Mater Rev*. 2016;61:20-25. doi: 10.1080/09506608.2015.1128310

45. Park KW, Truong TT, Park JH, et al. Robust and customizable spheroid culture system for regenerative medicine. *Biofabrication*. 2024;16:045016. doi: 10.1088/1758-5090/ad6795

46. Han SS, Cho Mo, Huh KM, Kang SW. Effects of nanopatterned-surface dishes on chondrocyte growth and cell progression. *RSC Adv*. 2021;11:39-47. doi: 10.1039/d0ra08256b

47. Han SS, Yoon HY, Yhee JY, et al. In situ cross-linkable hyaluronic acid hydrogels using copper free click chemistry for cartilage tissue engineering. *Polym Chem*. 2018;9:20-27. doi: 10.1039/C7PY01654A